Robust zero resistance in a superconducting high-entropy alloy at pressures up to 190 GPa

Jing Guo[a,1], Honghong Wang[a,b,1], Fabian von Rohr[c,1], Zhe Wang[a,b], Shu Cai[a,b], Yazhou Zhou[a,b], Ke Yang[d], Aiguo Li[d], Sheng Jiang[d], Qi Wu[a], Robert J. Cava[c,2], and Liling Sun[a,b,e,2]

[a]Institute of Physics, Chinese Academy of Sciences, Beijing 100190, China; [b]Department of Physics, University of Chinese Academy of Sciences, Beijing 100190, China; [c]Department of Chemistry, Princeton University, Princeton, NJ 08544; [d]Shanghai Synchrotron Radiation Facilities, Shanghai Institute of Applied Physics, Chinese Academy of Sciences, Shanghai 201204, China; and [e]Collaborative Innovation Center of Quantum Matter, Beijing, 100190, China

Contributed by Robert J. Cava, November 1, 2017 (sent for review September 27, 2017; reviewed by M. Brian Maple and Maw-Kuen Wu)

We report the observation of extraordinarily robust zero-resistance superconductivity in the pressurized $(TaNb)_{0.67}(HfZrTi)_{0.33}$ high-entropy alloy—a material with a body-centered-cubic crystal structure made from five randomly distributed transition-metal elements. The transition to superconductivity (T_C) increases from an initial temperature of 7.7 K at ambient pressure to 10 K at ∼60 GPa, and then slowly decreases to 9 K by 190.6 GPa, a pressure that falls within that of the outer core of the earth. We infer that the continuous existence of the zero-resistance superconductivity from 1 atm up to such a high pressure requires a special combination of electronic and mechanical characteristics. This high-entropy alloy superconductor thus may have a bright future for applications under extreme conditions, and also poses a challenge for understanding the underlying quantum physics.

superconductivity | high pressure | high-entropy alloy

High-entropy alloys (HEAs) are a new class of materials that are composed of multiple transition-metal elements in equimolar or near-equimolar ratios (1, 2). The diverse elements in HEAs are arranged randomly on the crystallographic positions in a simple lattice, and thus have been referred to as a metallic glass on an ordered lattice. By applying this concept, many HEAs have been found in disordered solid-solution phases with body-centered-cubic, hexagonal closest-packed, and face-centered-cubic crystal structures (3–6).

In many respects, HEAs display novel properties, including ultrahigh fracture toughness at cryogenic temperatures (7, 8), excellent specific strength (9), and superior mechanical performance at high temperatures (10). In addition to their promising mechanical properties, some HEAs also exhibit interesting electronic properties: $[TaNb]_{1-x}(ZrHfTi)_x$ HEAs were found to display superconductivity, for example (11, 12). The combination of the promising physical properties found in the HEAs points to great potential for application.

Pressure is one of the variables that can uncover unexpected phenomena and properties (13–16). For superconductors in particular, the pressure-induced enhancement of critical transition temperatures in copper-oxide and iron-pnictide superconductors (17–20), the reemergence of superconductivity in the alkaline iron selenide (21) and heavy fermion superconductors (22), pressure-induced superconductivity in H_3S (23–25) and elements (26, 27), are examples. Therefore, looking for new phenomena in the superconducting HEA under pressure is of great interest. Here we report high-pressure studies on the superconducting HEA $(TaNb)_{0.67}(HfZrTi)_{0.33}$, which has a critical transition temperature to the superconducting state (T_C) of about 7.8 K at ambient pressure (11, 12). Our observations demonstrate that this alloy exhibits extraordinarily robust superconductivity—its zero-resistance superconducting state is still achieved even at a pressure of 190.6 GPa, or almost 2 megabars (1 Mbar = 10^{11} pascal), a pressure like that within the outer core of the earth. Such a superconductor with a highly robust zero-resistance state, existing continuously from 1 atm to geological pressures, is extremely unusual and is in fact unique to the best of our knowledge. We attribute this surprising behavior to the stable crystal structure of the HEA combined with the apparent robustness of its electronic structure against very large amounts of lattice compression.

Results

Superconductivity Under Pressure. Fig. 1*A* shows the temperature dependence of the electrical resistance at ambient pressure for a $(TaNb)_{0.67}(HfZrTi)_{0.33}$ sample. A sharp drop to a zero-resistance superconducting state is observed at ∼7.7 K (we define T_C as the temperature where the resistance changes from a finite value to zero), consistent with the results reported in ref. 12. Applying a magnetic field on the sample shows that its superconducting transition temperature (T_C) systematically shifts to lower temperature (Fig. 1*A*, *Inset*), as expected. Temperature-dependent constant-current magnetic susceptibility characterization was also performed for the ambient-pressure sample. As shown in Fig. 1*B*, a strong diamagnetic response is observed starting at 7.6 K, indicative of a bulk superconducting nature.

High-pressure resistance measurements were performed for four samples that were cut from the material used as the standard for the superconductivity at ambient pressure. The electrical resistance measurements for these samples were performed between 4 and 300 K. Fig. 2*A* shows the temperature

Significance

High-entropy alloys (HEAs) are made from multiple transition-metal elements in equimolar or near-equimolar ratios. The elements in HEAs arrange themselves randomly on the crystallographic positions of a simple lattice. In addition to their excellent mechanical properties, one HEA has been reported to display superconductivity. In this work, we report that the Ta–Nb–Hf–Zr–Ti high-entropy alloy superconductor exhibits extraordinarily robust zero-resistance superconductivity under pressure up to 190.6 GPa. This is an observation of the zero-resistance state of a superconductor all the way from 1-bar pressure to the pressure of the earth's outer core without structure phase transition, making the superconducting HEA a promising candidate for new application under extreme condition.

Author contributions: R.J.C. and L.S. designed research; J.G., H.W., F.v.R., Z.W., S.C., Y.Z., K.Y., A.L., S.J., and L.S. performed research; J.G., H.W., F.v.R., Z.W., S.C., Y.Z., K.Y., A.L., S.J., Q.W., R.J.C., and L.S. analyzed data; and J.G., Q.W., R.J.C., and L.S. wrote the paper.

Reviewers: M.B.M., University of California, San Diego; and M.-K.W., Academia Sinica.

The authors declare no conflict of interest.

[1]J.G., H.W., and F.v.R. contributed equally to this work.

[2]To whom correspondence may be addressed. Email: rcava@princeton.edu or llsun@iphy.ac.cn.

This article contains supporting information online at www.pnas.org/lookup/suppl/doi:10.1073/pnas.1716981114/-/DCSupplemental.

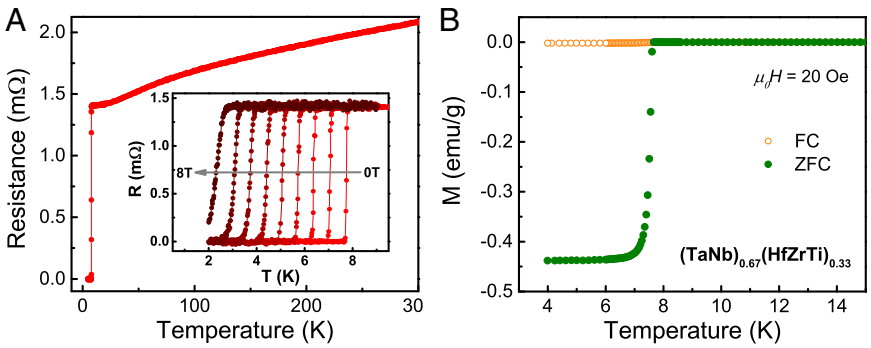

Fig. 1. Ambient-pressure properties of the superconducting HEA $(TaNb)_{0.67}(HfZrTi)_{0.33}$. (*A*) Resistance measured in the temperature range from 2 to 300 K. (*Inset*) Magnetic field dependence of the superconducting transition in fields from 0 to 8 T. (*B*) Zero-field cooling (ZFC) and field-cooling (FC) magnetization of the HEA in the vicinity of superconducting transition—the difference between the FC and ZFC curves is evidence for significant flux pinning on the material.

dependence of electrical resistance measured in the pressure range of 1.02–58.2 GPa for one of the samples. It is seen that the superconducting transitions of the sample subjected to different pressures are sharp and the zero-resistance state remains present throughout the full range of pressures applied. Zooming in on the resistance in the low-temperature regime

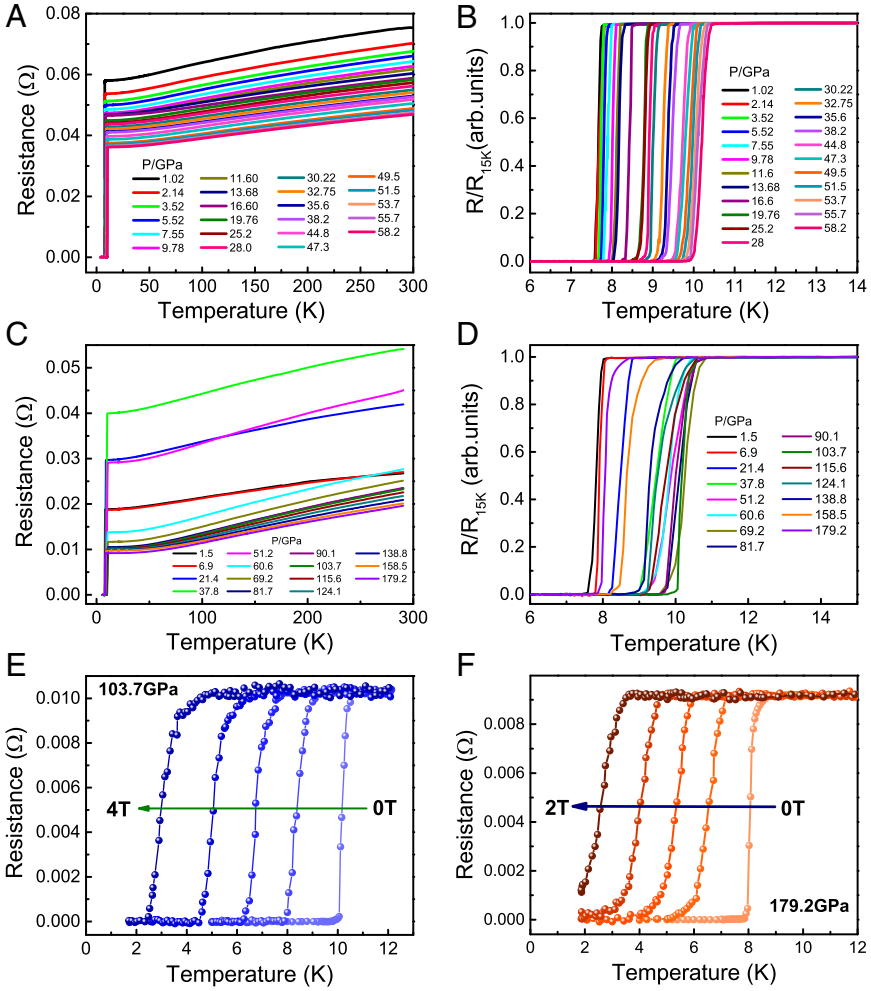

Fig. 2. Characterization of the superconducting transition of the HEA at high pressures. (*A*) Resistance versus temperature obtained from the measurements in the pressure range of 1.02–58.2 GPa, over a wide temperature range. (*B*) Detail of the normalized resistance at low temperatures for the data in *A*, clearly showing the effect of pressure on the resistance through the superconducting transition and the maintenance of the zero-resistance state over a very wide pressure range. (*C*) Temperature dependence of resistance measured on another sample in the pressure range of 1.5–179.2 GPa over a wide pressure range. (*D*) Enlarged view of normalized resistance in *C*, illustrating the superconducting transition at different pressures and in particular the robust zero-resistance state up to the pressure of 179.2 GPa. (*E* and *F*) Magnetic field dependence of the superconducting transition in the HEA at 103.7 and 179.2 GPa, respectively.

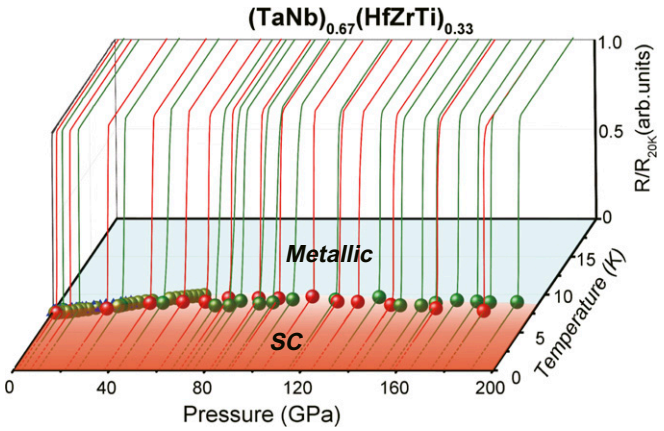

Fig. 3. Phase diagram of superconducting transition temperature vs. applied pressure up to 190.6 GPa for the HEA, combined with plots of the corresponding resistance vs. temperature. Blue triangles and dark-yellow balls in the diagram represent the zero-resistance superconducting transition temperature T_C obtained from measurements at pressure below 60 GPa, while the red and olive balls stand for zero-resistance T_C from the measurements at pressures up to 179.2 and 190.6 GPa, respectively.

(Fig. 2*B*), we find that the superconducting transition temperature T_C shifts to higher temperature upon increasing pressure. Consistent results are obtained from another sample in the pressure range of 0.3–30.1 GPa, as shown in Fig. 3. To investigate the superconducting behavior at higher pressures, we carried out resistance measurements for the third sample over the wide pressure range of 1.5–179.2 GPa (Fig. 2 *C* and *D*). As shown in Fig. 2*C*, the superconducting state still survives at a pressure as high as 179.2 GPa. Surprisingly, the zero-resistance state still exists at this high pressure (Fig. 2*D*). The magnetic field dependence of the superconducting transition measured at 103.7 and 179.2 GPa, respectively, further confirms the superconducting nature (Fig. 2 *E* and *F*). Furthermore, our measurements up to 190.6 GPa on the fourth sample show the reproducibility of the results (Fig. 3). This is an unusual behavior of such robust zero-resistance superconductivity in a material from 1 atm up to near 2 Mbar, a pressure found inside the outer core of the earth.

Pressure–Temperature Phase Diagram. We summarize our experimental results, obtained from samples measured in the four independent runs, in the pressure–temperature phase diagram shown in Fig. 3. It is seen that the 1-atm superconducting T_Cs of these samples are almost the same at ∼7.7 K, different from the T_C of any element included in the superconducting HEA investigated (28, 29) and clearly shown in previous studies to be a bulk property of the HEA (11, 12). T_C increases with pressure for the $(TaNb)_{0.67}(HfZrTi)_{0.33}$ HEA, exhibiting a slow increase from its ambient-pressure value of ∼7.7 to 10 K at ∼60 GPa. On further increasing the pressure, T_C remains almost unchanged until ∼100 GPa and then shows a slight decline until the pressure of 190.6 GPa, where the T_C is about 9 K. Attempts to apply an even higher pressure than 190.6 GPa led to breaking of the diamonds in the pressure cell, unfortunately, so we do not know whether the zero-resistance state survives to the pressure of the earth's inner core.

Discussion

High-pressure synchrotron X-ray diffraction (XRD) measurements on the $(TaNb)_{0.67}(HfZrTi)_{0.33}$ HEA were performed at

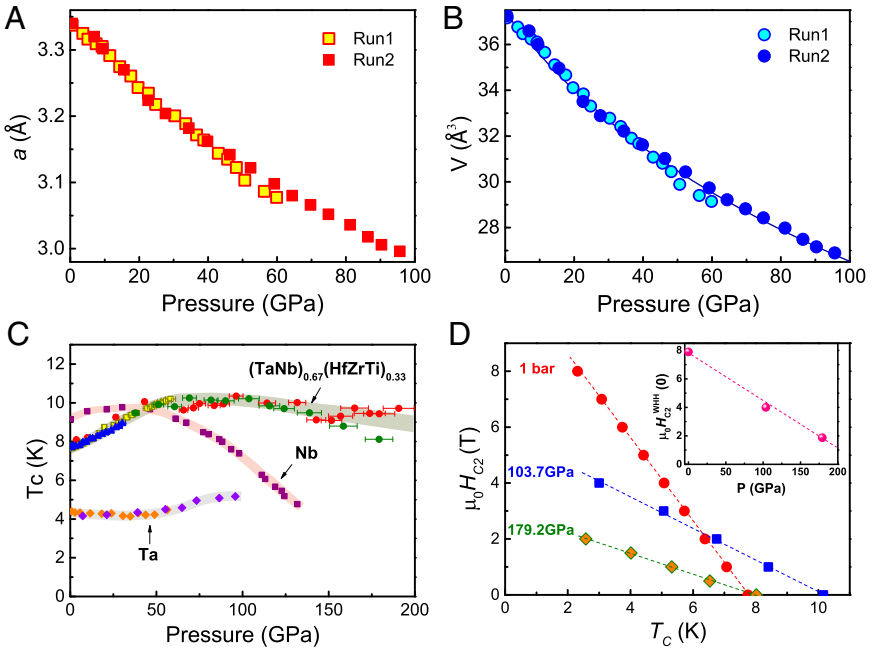

Fig. 4. Details of the high-pressure structure and superconductivity information for the superconducting HEA $(TaNb)_{0.67}(HfZrTi)_{0.33}$ and comparison with the behavior of constituent elements. (*A* and *B*) Pressure dependence of the lattice parameter and unit cell volume extracted from two independent XRD experiments. The SD for the lattice parameters obtained from the diffraction data are ∼1%. (*C*) The pressure-dependent change in the superconducting transition temperature of the HEA compared with those of Nb and Ta, its major elemental constituents. To make a better comparison with the reported T_C of elemental Nb (determined by magnetic susceptibility measurements, ref. 28), we use the midpoint T_C of our HEA and Ta samples in *C*. The solid circles, blue triangles, and yellow squares are the data for the HEA obtained in this study, the purple squares and orange diamonds are the data previously reported for elemental Nb (28) and Ta (29), respectively, and the violet diamonds are the data for elemental Ta found in this study. (*D*) Superconducting upper critical field H_{c2} as a function of temperature for the HEA at ambient pressure and pressures of 103.7 and 179.2 GPa. The dashed lines represent the slopes of the upper critical fields $(dH_{c2}/dT)_{T=T_C}$ at different pressures. (*Inset*) Pressure dependence of the zero-temperature upper critical field $H_{c2}(0)$ for the HEA superconductor up to ∼180 GPa.

beamline 15U of the Shanghai Synchrotron Radiation Facility. The results of two independent experiments show that the superconducting HEA does not undergo a structural phase transition up to pressures of ~96 GPa where the volume is compressed by ~28% (Fig. 4 *A* and *B* and Fig. S1), but its body-centered-cubic (bcc) structure is still maintained. Further, if the change of the volume is linearly extrapolated up to 190 GPa from 60 GPa, the volume is compressed by ~53%.

An analysis of the data (Fig. 4*C*) shows that the pressure dependence of the superconducting critical temperature T_C of the bcc superconducting HEA $(TaNb)_{0.67}(HfZrTi)_{0.33}$ is quite distinct from those of the bcc superconductors Nb and Ta, which are the major elemental constituents of the HEA material. [The superconducting T_C of elemental Ta has been measured to higher pressures than are found in the literature as part of the current study (Fig. S2)]. The T_C of the HEA superconductor continuously increases up to 96 GPa, distinct from what is observed in both Nb and Ta in the course of their exposure to pressure (28, 29). Thus, the superconducting HEA $(TaNb)_{0.67}(HfZrTi)_{0.33}$ is clearly distinct, and not just a diluted form of Nb or Ta.

To further evaluate the potential applicability of the HEA superconductor under extreme conditions, we also estimate the value of the upper critical magnetic field (H_{c2}, the magnetic field at which superconductivity disappears) for the pressurized material by using the Werthamer–Helfand–Hohenberg (WHH) formula (30):

$$H_{c2}^{\mathrm{WHH}}(0) = -0.693 T_C (dH_{c2}/dT)_{T=Tc}.$$

Fig. 4*D* shows a plot of H_{c2} versus T_C obtained at different pressures. The dashed lines represent the slopes of the upper critical fields $(dH_{c2}/dT)_{T = Tc}$ at different pressures. The estimated values of the upper critical fields at zero temperature are ~8 T at ambient pressure, ~4 T at 100 GPa, and ~2 T at 179.2 GPa (Fig. 4*D*, *Inset*). The very robust zero-resistance state and robust upper critical fields from ambient pressure to pressures as high as that of the earth's outer core, together with the high compressibility (the volume is compressed by ~28% at 96 GPa, and the linear extrapolated change of the volume up to 190 GPa from 60 GPa is ~53%), make the superconducting HEA a promising candidate for new applications and also pose a challenge for verifying the known superconductivity theory and developing a new one.

Materials and Methods

The sample was prepared from pieces of the pure metals. Stoichiometric amounts of niobium (purity 99.8%), tantalum (purity 99.9%), zirconium (purity 99.6%), hafnium (purity 99.6%), and titanium (purity 99.95%) pieces were arc melted in high currents ($T > 2{,}500$ °C) in an argon atmosphere and rapidly cooled on a water-chilled copper plate. A zirconium sponge was coheated to purify the reaction atmosphere from remaining oxygen. The samples were melted five times and turned over each time to ensure optimal mixing of the constituents (12). The elemental Ta for the comparison measurements had a purity of 99.95% with an ambient pressure T_C of 4.48 K.

High-pressure resistance and magnetoresistance measurements were carried out in a diamond-anvil cell made of Be–Cu alloy. The four-probe method was applied on the flat plane of the sample. Diamond anvils with 300-, 50-, and 40-μm flats were used for different independent measurements; smaller flats were used for the higher-pressure measurements. An appropriate amount of NaCl powder was employed as the pressure-transmitting medium for the two runs of lower-pressure experiments, while no pressure medium was employed for the two runs of higher-pressure (near 2 Mbar) experiments. Pressures below and above 60 GPa were determined by the ruby fluorescence method (31) and the pressure dependence of the diamond Raman shift method (32, 33), respectively.

Two independent runs of high-pressure XRD measurements were carried out at beamline 15U at the Shanghai Synchrotron Radiation Facility. Pressure was applied up to ~60 GPa for the first-run measurements and ~96 GPa for the second-run measurements. Diamonds with flats of 300 and 200 μm were used and a monochromatic X-ray beam with a wavelength of 0.6199 Å was employed for all of the measurements. The pressures were determined by the ruby fluorescence method (31) and the pressure-dependent diamond Raman shift method (32, 33).

ACKNOWLEDGMENTS. The work in China was supported by the National Key Research and Development Program of China (Grants 2017YFA0302900, 2016YFA0300300, and 2017YFA0303103), the NSF of China (Grants 91321207, 11427805, U1532267, and 11604376), and the Strategic Priority Research Program (B) of the Chinese Academy of Sciences (Grant XDB07020300). The work at Princeton was supported by the Gordon and Betty Moore Foundation EPiQS initiative, Grant GBMF-4412.

1. Yeh J-W, et al. (2004) Nanostructured high-entropy alloys with multiple principal elements: Novel alloy design concepts and outcomes. *Adv Eng Mater* 6:299–303.
2. Yeh J-W (2006) Recent progress in high entropy alloys. *Ann Chimie Sci Materiaux* 31: 633–648.
3. Ye Y, Wang Q, Lu J, Liu CT, Yang Y (2016) High-entropy alloy: Challenges and prospects. *Mater Today* 19:349–362.
4. Yeh J-W (2013) Alloy design strategies and future trends in high-entropy alloys. *JOM* 65:1759–1771.
5. Urban K, Feuerbacher M (2004) Structurally complex alloy phases. *J Non-Cryst Solids* 334:143–150.
6. Senkov ON, Miller JD, Miracle DB, Woodward C (2015) Accelerated exploration of multi-principal element alloys with solid solution phases. *Nat Commun* 6:6529.
7. Gludovatz B, et al. (2016) Exceptional damage-tolerance of a medium-entropy alloy CrCoNi at cryogenic temperatures. *Nat Commun* 7:10602.
8. Gludovatz B, et al. (2014) A fracture-resistant high-entropy alloy for cryogenic applications. *Science* 345:1153–1158.
9. Kou H, Lu J, Li Y (2014) High-strength and high-ductility nanostructured and amorphous metallic materials. *Adv Mater* 26:5518–5524.
10. Zou Y, Ma H, Spolenak R (2015) Ultrastrong ductile and stable high-entropy alloys at small scales. *Nat Commun* 6:7748.
11. Koželj P, et al. (2014) Discovery of a superconducting high-entropy alloy. *Phys Rev Lett* 113:107001.
12. von Rohr F, Winiarski MJ, Tao J, Klimczuk T, Cava RJ (2016) Effect of electron count and chemical complexity in the Ta-Nb-Hf-Zr-Ti high-entropy alloy superconductor. *Proc Natl Acad Sci USA* 113:E7144–E7150.
13. Hemley RJ, Ashcroft NW (1998) The revealing role of pressure in the condensed matter sciences. *Phys Today* 51:26–32.
14. Mao H-K, et al. (2016) Recent advances in high-pressure science and technology. *Matter Radiat Extremes* 1:59–75.
15. Dias RP, Silvera IF (2017) Observation of the Wigner-Huntington transition to metallic hydrogen. *Science* 355:715–718.
16. Ma Y, et al. (2009) Transparent dense sodium. *Nature* 458:182–185.
17. Chu CW, et al. (1993) Superconductivity above 150 K in $HgBa_2Ca_2Cu_3O_{8+\delta}$ at high pressure. *Nature* 365:323–325.
18. Chen X-J, et al. (2010) Enhancement of superconductivity by pressure-driven competition in electronic order. *Nature* 466:950–953.
19. Takahashi H, et al. (2008) Superconductivity at 43 K in an iron-based layered compound $LaO_{(1-x)}F_{(x)}FeAs$. *Nature* 453:376–378.
20. Medvedev S, et al. (2009) Electronic and magnetic phase diagram of β-$Fe_{(1.01)}Se$ with superconductivity at 36.7 K under pressure. *Nat Mater* 8:630–633.
21. Sun L, et al. (2012) Re-emerging superconductivity at 48 kelvin in iron chalcogenides. *Nature* 483:67–69.
22. Yuan HQ, et al. (2003) Observation of two distinct superconducting phases in $CeCu_2Si_2$. *Science* 302:2104–2107.
23. Duan D, et al. (2014) Pressure-induced metallization of dense $(H_2S)_2H_2$ with high-Tc superconductivity. *Sci Rep* 4:6968.
24. Drozdov AP, Eremets MI, Troyan IA, Ksenofontov V, Shylin SI (2015) Conventional superconductivity at 203 kelvin at high pressures in the sulfur hydride system. *Nature* 525:73–76.
25. Troyan I, et al. (2016) Observation of superconductivity in hydrogen sulfide from nuclear resonant scattering. *Science* 351:1303–1306.
26. Shimizu K, Ishikawa H, Takao D, Yagi T, Amaya K (2002) Superconductivity in compressed lithium at 20 K. *Nature* 419:597–599.
27. Hamlin JJ (2015) Superconductivity in the metallic elements at high pressures. *Phys C* 514:59–76.
28. Struzhkin VV, Timofeev YA, Hemley RJ, Mao HK (1997) Superconducting Tc and electron-phonon coupling in Nb to 132 GPa: Magnetic susceptibility at megabar pressures. *Phys Rev Lett* 79:4262–4265.
29. Tonkov EY, Ponyatovsky E (2004) *Phase Transformations of Elements Under High Pressure* (CRC Press LLC, Boca Raton, FL), pp 237–239.
30. Werthamer NR, Helfand E, Hohenberg PC (1966) Temperature and purity dependence of the superconducting critical field. *Phys Rev* 147:295–302.
31. Mao HK, Xu J, Bell PM (1986) Calibration of the ruby pressure gauge to 800 kbar under quasi-hydrostatic conditions. *J Geophys Res* 91:4673–4676.
32. Sun LL, Ruoff AL, Stupian G (2006) Convenient optical pressure gauge for multi-megabar pressures calibrated to 300 GPa. *Appl Phys Lett* 86:014103.
33. Akahama Y, Kawamura H (2006) Pressure calibration of diamond anvil Raman gauge to 310 GPa. *J Appl Phys* 100:043516.